

Article

Microstructure and Strengthening-Toughening Mechanism of Nitrogen-Alloyed 4Cr5Mo2V Hot-Working Die Steel

Jinbo Gu ¹, Jingyuan Li ^{1,*} and Yulai Chen ²

¹ School of Materials Science and Engineering, University of Science & Technology, Beijing 100083, China; gujinboustb@163.com

² Engineering Research Institute, University of Science & Technology Beijing, Beijing 100083, China; yulaic@ustb.edu.cn

* Correspondence: lijy@ustb.edu.cn; Tel.: +86-010-8237-6939

Received: 27 June 2017; Accepted: 10 August 2017; Published: 14 August 2017

Abstract: The microstructure and strengthening-toughening mechanism of a modified 4Cr5Mo2V hot-working die steel with nitrogen (0.08% N) were investigated using hardness and toughness measurements, optical microscopy, scanning electron microscopy, X-ray diffraction experiments, transmission electron microscopy, and dilatometry. The results showed that the nitrogen addition could increase the hardness and temperability of 4Cr5Mo2V steel without toughness loss with a suitable heat treatment procedure. The fair match of high strength and toughness of the nitrogen-alloyed 4Cr5Mo2V steel is associated with the refinement of the prior austenite grain, the solution hardening of nitrogen atoms, and the increase of retained austenite. Before quenching, nitrogen tends to precipitate in the form of a large amount of undissolved finer V(C, N), imposing a stronger effect on restricting the growth of prior austenitic grains and increasing the grain refining efficiency of VC by 6.8 times according to an estimate. During the quenching process, the nitrogen decreases the M_s of the martensitic transformation, increasing retained austenite, which is a benefit for toughness. During the tempering process, some of the N atoms in M(C, N) were dissolved in the matrix, causing crystal lattice distortions, thus boosting the solution reinforcing effect. Meanwhile, the solid-dissolved nitrogen inhibits the diffusion of carbon, decreasing the growth rate of the carbides and increasing tempering resistance.

Keywords: strengthening-toughening; nitrogen-alloyed; hot-working die steel; precipitates

1. Introduction

Die steel 4Cr5Mo2V (Uddeholm designation DIEVAR) is a low silicon and high molybdenum hot-work tool steel developed from H13 die steel specifically for the sake of better heat checking resistance and gross cracking resistance [1]. Due to excellent hot strength and toughness, it is increasingly employed in forging, hot-extrusion, and die-casting. In the case of the ever-growing requirements of industrial applications, better-quality tool steel is continually needed to increase the service life of tool steel. Many studies have illustrated the great interest in improving the performance of die steel [2–4]. Improvement of properties of tool steels can be achieved through improving the hardness and toughness by adjusting the constituents or optimization of the production technology such as a deep cryogenic treatment [5,6]. Several new trends in optimizing chemical composition such as Nb-microalloying or Rare Earth addition have been developed to improve the performance [7–9].

It has been acknowledged that nitrogen addition can strengthen Fe-based alloys and improve the properties of the steel [10,11]. With the implementation of high-pressure melting technology and the higher nitrogen content in steel, the effect of nitrogen on the microstructure and the properties of

steel have been investigated thoroughly, especially in austenitic stainless steel [12]. Simmons et al., suggested that nitrogen plays a more effective role in solution strengthening and grain refinement than carbon [13]. Werner et al. reported that nitrogen can obviously increase the strength of austenitic stainless steels without a significant loss of ductility or impact toughness of the steel [14]. Behjati et al. demonstrated that the nitrogen existing as a solution element is much more effective than that existing in the form of carbonitrides, since carbonitrides have a harmful effect on impact toughness [15]. However, there have been few reports on nitrogen-alloyed die steel. In the present study, a new type of nitrogen-alloyed H13 hot-work die steel was investigated. Nitrogen alloying improved the hardness of H13 die steel with no reduction in toughness [16]. However, the strengthening-toughening mechanism needs further clarification. In addition, whether the improvement can be applied to 4Cr5Mo2V die steel with a higher amount of nitrogen needs further confirmation.

Hence, the aim of this work was to investigate the effect of nitrogen on the microstructure of 4Cr5Mo2V steel during the heat treatment process. Meanwhile, the strengthening-toughening mechanism of nitrogen-alloyed 4Cr5Mo2V hot-working die steel was further clarified.

2. Materials and Methods

Two 25 kg ingots of 4Cr5Mo2V steel with the composition listed in Table 1 were prepared using a vacuum induction furnace (Jinzhou Boda Co., Ltd., Jinzhou, China). The nitrogen-alloyed steel was melted under the protection of a nitrogen atmosphere of 0.6 MPa and nitrogen was added during the smelting process in the form of a nitrogen-containing ferrochromium alloy. The ingot was homogenized at 1250 °C for 3 h, multi-directional hot-forged at a temperature range of 850–1150 °C, and then air-cooled to ambient temperature.

Table 1. Chemical compositions of tested steel (wt %).

Element	C	Si	Mn	Cr	Mo	V	N ¹
Nitrogen steel	0.33	0.5	0.42	5.3	2.4	0.68	0.08
Nitrogen-free steel	0.33	0.5	0.40	5.4	2.4	0.63	-

¹ Nitrogen content was measured by thermal the conductometric method after fusion in a current of argon gas. The other metallic elements were measured by chemical titration.

Specimens, for spheroidizing annealing (SA), quenching, and the tempering process, measuring $15 \times 15 \times 15 \text{ mm}^3$ were taken from the hot forged samples. During SA, the nitrogen-alloyed 4Cr5Mo2V samples were heated to 850 °C and cooled to below 650 °C at a rate of $10 \text{ °C} \cdot \text{h}^{-1}$ in the furnace, whereupon it was then taken out of the furnace and cooled to ambient temperature. Subsequently, during the quenching process, the samples were reheated to and kept at 1000 °C, 1030 °C for 0.5 h, respectively. Thereafter, the samples were oil-quenched to ambient temperature. Finally, the quenched samples were tempered at 580 °C, 600 °C, and 650 °C for 2, 4, 6 h, respectively. The heat-treating process is as shown in Figure 1.

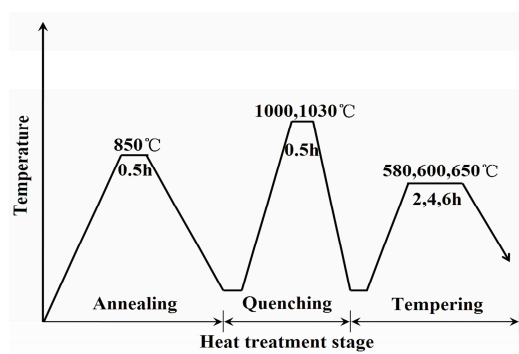


Figure 1. Heat-treatment regime of samples.

Samples with a hardness of more than 48 HRC, which were higher than the hardness of ordinary 4Cr5Mo2V die steel, were selected to subsequently test for impact toughness to obtain an optimum heat treatment. The specimens for impact toughness test were $11 \times 11 \times 60 \text{ mm}^3$ square bars cut from forgings. Then, the nitrogen-alloyed steel and nitrogen-free steel were subjected to the optimum heat treatment with different tempering times ranging from 0 h to 8 h to compare the tempering stability.

The HRC hardness of samples was measured using a TH320 Rockwell Hardness Tester (Beijing Time Group Co., Ltd., Beijing, China) at five points on each sample and the mean value was calculated (ASTM E18-15). The impact toughness of the heat-treated sample was tested in a JB-30B impact testing machine (Jinan Hensgrand instrument Co., Ltd., Jinan, China) using the Charpy V-notch test method (ASTM A370). The microstructures of the samples were characterized on an optical microscope (DM2500M, Leica Camera AG, Wetzlar, Germany) after mechanical polishing and etching in an 8% nital solution. The average grain size and martensite lath size were measured with SISC IAS V8.0 image software [17] according to the standard linear intercept method [18]. Five dispersive martensite packets were chosen to calculate the average martensite lath size.

The morphology of the precipitates was investigated by carbon extraction replica [19] on Cu-grids and a transmission electron microscope (J EM-2000FX, JEOL, Tokyo, Japan). To obtain the mean size of precipitates accurately, 100 particles were selected randomly from five pieces of the pictures of $30 \mu\text{m}^2$ (large visual field) and five pieces of the pictures of $10 \mu\text{m}^2$ (small visual field).

To capture the conversion points of the martensitic transformation, dilatometric measurements were conducted on a dilatometer (DIL805A, Baehr, Pirmasens, Germany) using 4 mm diameter \times 10 mm cylindrical specimens. The conversion points of the martensitic transformation were analyzed from the dilatometry curve using the tangent method [20].

Finally, the lattice distortion of the samples was investigated by X-ray diffraction (DMAX-RB, Rigaku, Tokyo, Japan) at a step of 0.01° and a counting time of 1 s/step using $12 \times 12 \times 12 \text{ mm}^3$ samples. The equilibrium fraction of the precipitates was calculated using Thermo-Calc software (TCFE7 database, Thermo-Calc Software, Solna, Sweden).

3. Results

3.1. Mechanical Properties

The test results of the mechanical properties are as shown in Table 2. As can be seen, the nitrogen-alloyed steel can achieve approximately the same toughness as that of nitrogen-free steel, while the hardness of nitrogen-alloyed steel is about 2 HRC higher than that of nitrogen-free steel. Especially, the nitrogen-alloy steel can achieve a toughness of $14.3 \text{ J}\cdot\text{cm}^{-2}$ and hardness of 49.6 HRC when tempering at 600°C for 4 h. The experimental results indicated that nitrogen-alloyed 4Cr5Mo2V steel can obtain a better match of hardness and toughness with the suitable heat treatment procedure.

Table 2. Mechanical parameters after tempering.

Quenching Tempering	1000 °C/0.5 h		1030 °C/0.5 h		
	580 °C/6 h	600 °C/2 h	600 °C/2 h	600 °C/4 h	600 °C/6 h
	Nitrogen-alloyed steel/Nitrogen-free steel				
Average hardness ¹ /HRC	50.2/48.2	49.7/48.1	51.0/48.6	49.6/47.3	48.0/46.0
Average impact toughness ¹ (ak/J·cm ⁻²)	12.3/12.6	12.5/12.5	12.0/12.3	14.3/14.4	14.6/14.8

¹ The experimental errors are ± 1 HRC and $\pm 0.5 \text{ J}\cdot\text{cm}^{-2}$ for hardness and toughness values.

Nitrogen-alloyed and nitrogen-free steel exhibited different tempering stability, as shown in Figure 2. As can be seen, the initial hardness of both samples at the quenched state was very similar at about 54–55 HRC, and the hardness of both decreased continuously with the holding time. However, the difference was that the hardness of the nitrogen-alloyed steel decreased more slowly than that of the nitrogen-free steel. After tempering at 600°C for 8 h, the hardness of the nitrogen-alloyed steel

dropped to 47 HRC while that of the nitrogen-free steel was 45 HRC, which indicated that nitrogen improved the temper stability of the steel.

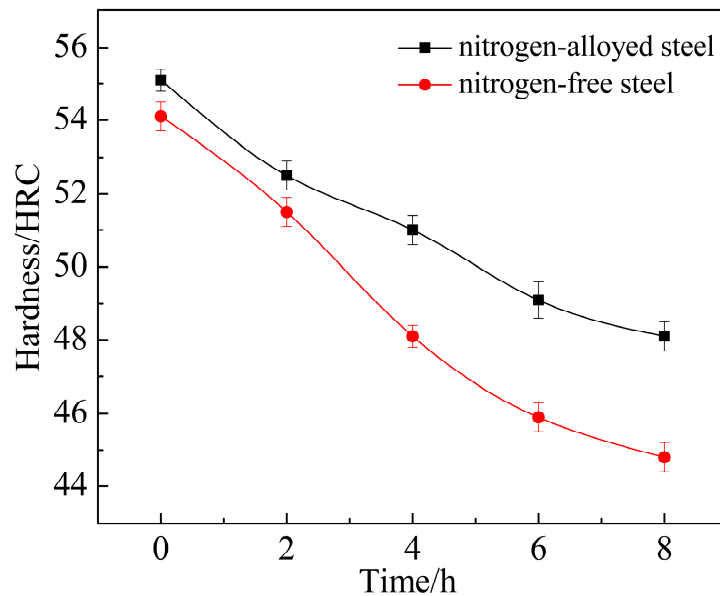


Figure 2. Hardness of tested steel tempered at 600 °C for various holding times.

3.2. Martensite

Figure 3 shows the metallographic structure of the samples subjected to austenitization at 1030 °C for 30 min followed by tempering at 600 °C for 2 h, 4 h and tempering at 650 °C for 4 h. As can be seen, the microstructures of both samples are similar and mainly consist of lath-like martensite (marked as “M”) as well as a small amount of remaining austenite. Notably, the prior austenite grain boundary is visible. Clearly, the martensite lath of nitrogen-alloyed steel is much narrower and shorter than that of nitrogen-free steel. Moreover, the prior austenite grain size of the two steels is much different. Taking samples tempered at 600 °C (2 h) for example, the average prior austenite grain diameter was about 15 μm and 25 μm for nitrogen-alloyed steel and nitrogen-free steel, respectively.

With the increase of tempering temperature or tempering time, the width of the martensite lath evidently increases, indicating the recovery of the martensitic matrix. However, lath-like martensite of nitrogen-alloyed steel exhibits a slightly narrower and shorter appearance than that of nitrogen-free steel, when both sets of samples received the same subsequent quenching and tempering treatments. The coarsening of martensite lath in nitrogen-alloyed steel is far less than that of nitrogen-free steel. For example, the average thicknesses of martensite lath in steels tempered at 600 °C for 4 h were about 0.2 μm and 0.3 μm for nitrogen-alloyed steel and nitrogen-free steel, respectively. By contrast, they were 0.3 μm and 0.5 μm for nitrogen-alloyed steel and nitrogen-free steel when the samples were tempered at 650 °C for 4 h. The coarsening rate of martensite is related to the pinning effect of finer precipitates such as MC and M₆C on the movement of lath boundaries. It can be deduced that the addition of nitrogen inhibits the recovery of the martensitic matrix by refining the precipitates during the tempering process [21,22].

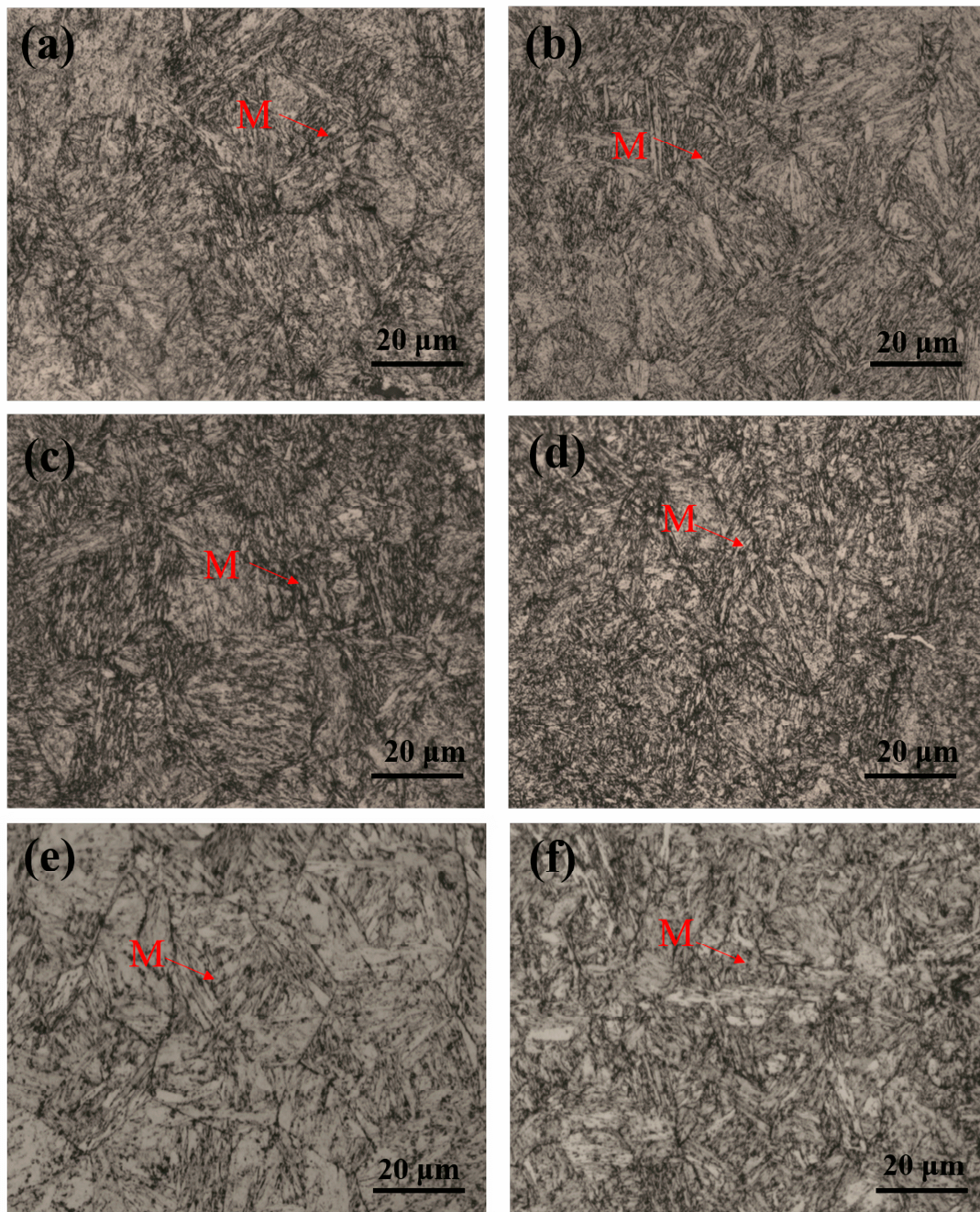


Figure 3. Metallographic images of tested steel after tempering: (a) Nitrogen-free steel (600 °C for 2 h); (b) nitrogen-alloyed steel (600 °C for 2 h); (c) nitrogen-free steel (600 °C for 4 h); (d) nitrogen-alloyed steel (600 °C for 4 h); (e) nitrogen-free steel (650 °C for 4 h); (f) nitrogen-alloyed steel (650 °C for 4 h).

3.3. Precipitates

Previous studies have shown that the properties of steel are closely related to the size, shape, and volume fraction of the precipitates [23–28]. Moreover, the added nitrogen has an effect on the evolution of precipitates at different stages of the heat treatment. Figure 4 shows transmission electron microscope (TEM) images of precipitates in the quenched specimens. Clearly, larger amounts of undissolved dispersed carbides were visible in nitrogen-alloyed steel. To investigate the chemical composition and crystal structure of the precipitates, the undissolved precipitates were analyzed with further calibration of the diffraction spot (lattice constant $a = b = c = 0.4154$ nm) and chemical

composition, and can be identified as V(C, N) with a fcc crystal structure, while the precipitates in nitrogen-free steel are confirmed as VC (lattice constant $a = b = c = 0.4182$ nm). Notably, the V(C, N) particles (20 nm in diameter) were much finer than those in nitrogen-free steel (50 nm in diameter). Apparently, nitrogen addition is effective to form finer V(C, N) particles, which are not easy to be coarsened [29]. Due to high thermal stability, most of the V(C, N) particles could not be dissolved during the heating stage of the quenching process. They may pin the prior austenite grain boundaries during the heat treatment process, thus refining the prior grains. The precipitation of finer V-rich M(C, N) plays a key role in ensuring the toughness of the steel.

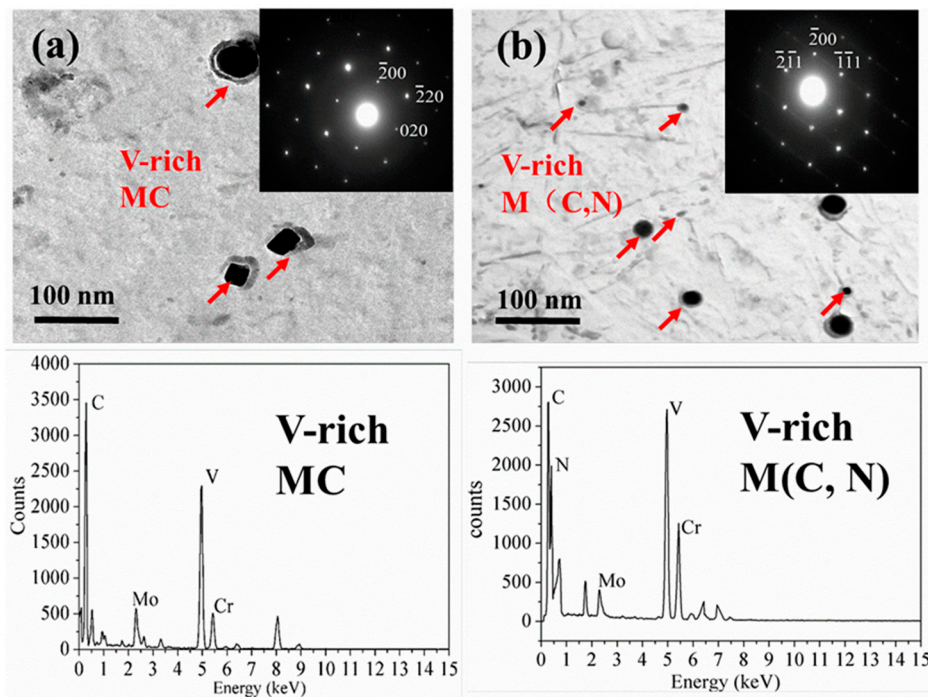


Figure 4. Transmission electron micrographs of the microstructure of the precipitates in samples at 1030 °C quenching temperature: (a) Nitrogen-free steel; (b) nitrogen-alloyed steel.

Figure 5 shows the precipitates tempered at 600 °C and 650 °C for 4 h. Obviously, the amount of precipitates in the samples is much more than in quenched samples, indicating that many precipitates such as M_6C and $M_{23}C_6$ were formed during the tempering process. It is important to note that, in the case of nitrogen-alloyed steel, a uniform distribution of much finer precipitates (ranging from 80 nm to 150 nm) occurs compared with the case of nitrogen-free steel (ranging from 100 nm to 200 nm). More remarkable, there are large amounts of dispersed and finer precipitates (average diameter 10 nm) identified as V(C, N) in nitrogen-alloyed steel, indicating that the nitrogen addition promoted the precipitation of vanadium. As can be seen from Figure 5c,d, the mean size of the precipitates becomes bigger with the increase of tempering temperature, but the coarsening rate of the precipitates in nitrogen-alloyed steel is much slower than that of nitrogen-free steel. Obviously, nitrogen addition inhibited the precipitation and coarsening of the precipitates during the tempering process. Furthermore, the finer precipitates in the nitrogen-alloyed steel had a stronger pinning effect on the movement of the lath boundary, thus decreasing the coarsening of martensite during the tempering process.

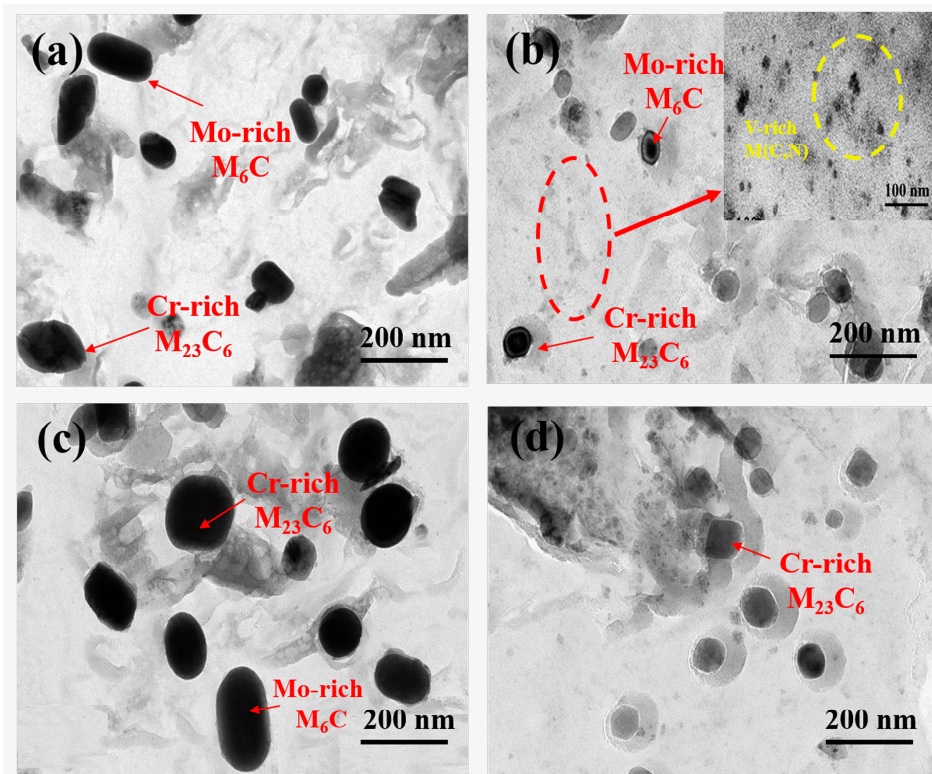


Figure 5. Bright-field transmission electron microscopy (TEM) micrographs of precipitates extracted from the specimen tempered at different temperature for 4 h: (a) Nitrogen-free steel (600 °C); (b) nitrogen-alloyed steel (600 °C); (c) nitrogen-free steel (650 °C); (d) nitrogen-alloyed steel (650 °C).

3.4. Lattice Distortion

Solid-dissolved nitrogen in the metallic matrix plays an important role in enhancing the solid solution strengthening effect which can be reflected by the lattice distortion of the matrix [30]. The results of the diffraction angle 2θ measurements from the X-ray diffraction (XRD) analysis display the lattice distortion of the Fe matrix, as shown in Figure 6. It has been definitely confirmed that the lattice distortion of the matrix can be characterized by $\Delta d/d\%$ of certain lattice planes [31]. In this paper, we choose $\Delta d/d\%$ of (110) to evaluate the matrix lattice distortion where d and Δd represent the interplanar distance (Dm) and the change of interplanar distance, respectively. The result is shown in Table 3. As can be seen, after the same heat-treated process, the lattice distortion of nitrogen steel is more obvious than that of nitrogen-free steel. Additionally, the lattice distortion of steel tempered at 600 °C is more severe than that at 650 °C.

In other words, the diffraction angles of the tested steels are shifted towards smaller diffraction angles compared to standard α -Fe. For example, the lattice plane (110) peaks are located at 44.15° and 44.50° for the nitrogen-alloyed and nitrogen-free steel tempered at 600 °C, respectively, and 44.40° and 44.55° for those at 650 °C, respectively although it is located at 44.66° for standard α -Fe [26]. This shift mainly results from an oversaturated body-centered cubic structure of martensite. A smaller diffraction angle indicates more bias and more lattice distortion [32]. The high concentration of interstitial elements such as C and N in the Fe matrix results in distorting the lattice of ferrite and thus the diffraction peaks of ferrite deviate to a small angle. Apparently, nitrogen addition increases the lattice distortion of the matrix, i.e., nitrogen enhances the solid solution strengthening effect of tempered steel. In addition, as the tempering temperature increases, the lattice distortion of the Fe matrix decreases as the amount of nitrogen existing as solid-solution state decreases, which is consistent with previous research [33].

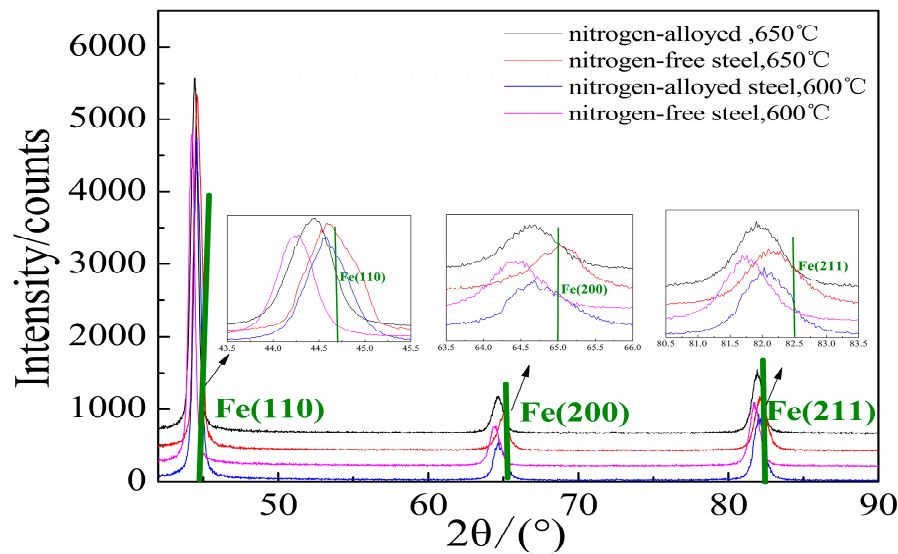


Figure 6. X-ray diffraction result showing the lattice distortion of tested steels quenched at 1030 °C and tempered at 600 °C and 650 °C for 4 h.

Table 3. Lattice distortion of samples quenched at 1030 °C for 0.5 h and tempered at 600 °C and 650 °C, respectively, for 4.0 h. (*Dm*: Interplanar distance.)

Samples	Tempering Temperature (°C)	Standard <i>Dm</i> (Å)	Mean <i>Dm</i> (Å)	Change ($\Delta d/d\%$)
Nitrogen-free	600	2.027	2.043	0.79
Nitrogen-alloyed	600	2.027	2.064	1.82
Nitrogen-free	650	2.027	2.037	0.50
Nitrogen-alloyed	650	2.027	2.056	1.43

4. Discussion

4.1. Effect of Nitrogen on Precipitates

Experimental results show that nitrogen alloyed in steel affects the precipitation and dissolving reaction of the tested steel significantly. The equilibrium formation of precipitates in steels was investigated using Thermo-Calc thermodynamic software (TCFE7 database, Thermo-Calc Software, Solna, Sweden), as shown in Figure 7. The type of carbide is defined in the Thermo-Calc database according to its stoichiometric formula. As can be seen from Figure 7a,b, complex and varied carbides such as MC-type, M_6C -type M_7C_3 -type and $M_{23}C_6$ -type precipitated at different temperatures in both samples, which is consistent with prior research [34–36]. To simplify issues here, two important temperatures (quenching temperature 1030 °C and tempering temperature 600 °C) were chosen to analyze the precipitation of two samples during the quenching and tempering process. Most of the precipitates are dissolved in matrix during the heating stage of the quenching process (1030 °C), except for a certain amount of MC-type carbides which are the most important strengthening carbides. However, it is apparent that the amount of undissolved MC in the nitrogen-alloyed steel (0.5%) is greater than that of nitrogen-free steel (0.2%). This suggests that the mergence of nitrogen into MC is conducive to the nucleation of MC resulting in a larger amount. Furthermore, the main elements of MC were also investigated. As shown in Figure 7c,d, MC exists mainly as VC in the nitrogen-free steel and as V(C, N) in nitrogen-alloyed steel. The reason may be that both C and N are available to form V-rich carbonitrides. It can be seen that the solid solution temperature of V(C, N) in the nitrogen-alloyed steel is 1300 °C while that of VC is 1050 °C. This signifies that the incorporation of nitrogen into MC could

lead V(C, N) to exist at higher temperature and thus impose important effects on refining the prior austenitic grains.

Subsequently, during the tempering treatment at 600 °C, a large amount of carbides such as $M_{23}C_6$ and M_6C precipitate in both samples, and there is no distinct difference in the amount of these carbides for the two tested steels. However, a subtle change of chemical composition occurs to MC of nitrogen-alloy steel. As shown in Figure 7c,d, the fraction of N atoms in V(C, N) decreases with the increasing fraction of C, indicating that some of the C atoms in the matrix would displace the N atoms of V(C, N) and most of the N would be as solid-dissolved in the matrix at 600 °C. N atoms and C atoms suppress the dispersion of one another in the process of the displacement reaction, and thus in refining the precipitates. Further, the solid-dissolved nitrogen in tempered steels would cause lattice distortion of the matrix, playing an important role in solution strengthening. The solid solution of nitrogen can be observed by XRD, as shown in Figure 6.

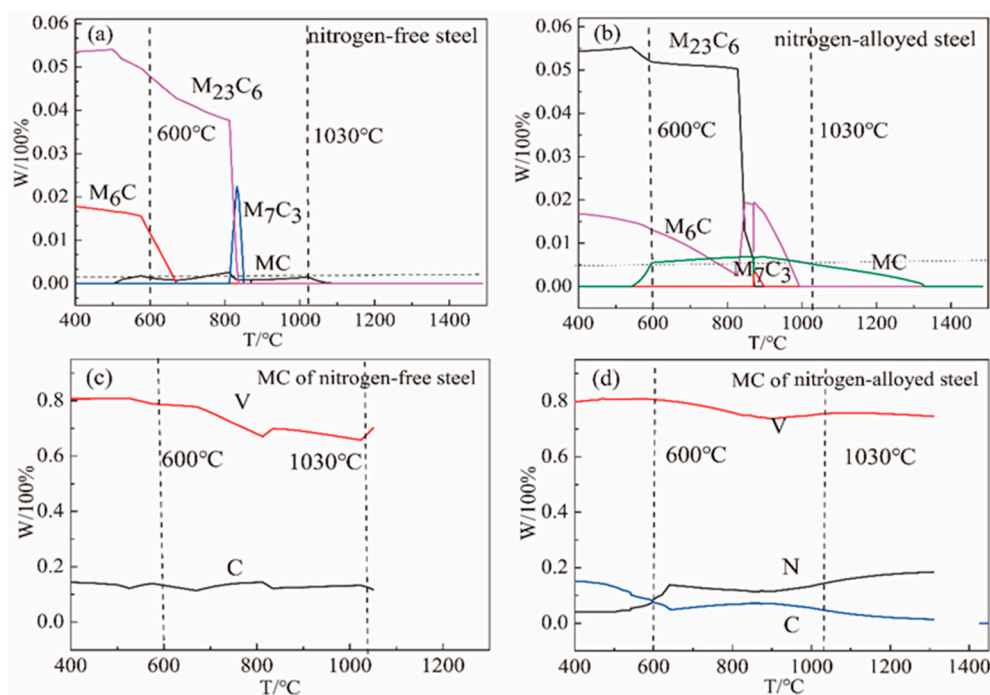


Figure 7. Equilibrium precipitation calculated by Thermo-Calc software for various carbides in samples (W: Weight percent in γ axis): (a) Nitrogen-free; and (b) nitrogen-alloyed steel; and for the elements of the MC carbide (c) nitrogen-free; (d) nitrogen-alloyed steel.

4.2. Effect of V(C, N) on Refining Prior Austenitic Grains

The finer grains could not only improve the hardness of the steel but also guaranteed toughness. Obviously, the effect of nitrogen on refining the grains plays an important role in obtaining optimum strength and toughness. The experimental results revealed that the grain refinement of nitrogen-alloyed steel is related to the precipitation of a much finer dispersion of the V(C, N) during the reheating process. This stronger pinning effect can be interpreted in terms of classical pinning theory in that the effect of precipitates on pinning the austenitic grain boundary is mainly related to the size and number of the precipitates and the interface structure between the austenite matrix and the precipitates. The effect of nitrogen on refining the prior austenitic grains could be estimated in the process as below. The required parameters of VC and V(C, N) are shown in Table 4. The lattice constant and diameter parameter of the VC and V(C, N) particles are analyzed from TEM images of the precipitates of the quenched samples. The volume fraction f , of VC and V(C, N) was calculated by the Thermo-Calc software, valued as 0.68% and 0.21% for nitrogen-alloyed steel and nitrogen-free steel, respectively.

Table 4. Parameters of VC and V(C, N) in the tested samples.

Precipitates	Lattice Constant (nm)	Average Diameter ¹ (nm)	Volume Fraction (f)
VC	0.4182	50	0.21%
V(C, N)	0.4154	20	0.68%

¹ The standard deviation values of diameter are 10 nm and 8 nm for VC and V(C, N).

The behavior of MC during the heating process is closely related to lattice misfit and the interfacial energy of the MC/matrix system. The lattice misfit parameter δ which is defined as the relative difference of lattice width can be obtained as follows [37]:

$$\delta = \left| \frac{a_{M(C, N)} - a_{\gamma}}{a_{M(C, N)}} \right|, \quad (1)$$

$$a_{\gamma} = 0.36468 \times [1 + 21.1 \times 10^{-6}(T - 912)] + 0.0033[C], \quad (2)$$

where $a_{M(C, N)}$ and a_{γ} are the lattice constants of M(C, N) and austenite, respectively. T is temperature and $[C]$ is carbon content in the matrix. The lattice constants of M(C, N) are valued as 0.4182 nm and 0.4154 nm for VC and V(C, N), respectively. The interface energy, σ , of a semi-coherent interface [37] can be calculated from Equations (3)–(5):

$$\sigma = \frac{E_{\gamma} a_{\gamma}}{4\sqrt{2}\pi(1 - \theta^2)}, \quad (3)$$

$$E_{\gamma} = 254680 - 114.76T, \quad (4)$$

$$f(\delta) = \delta \left(\ln \frac{1}{2\delta} + \frac{2}{1 + \frac{1}{4\delta^2}} \right), \quad (5)$$

where E_{γ} is Young's modulus, which can be calculated from Equation (4), θ is the Poisson ratio of austenite, valued as 0.32. The maximum encumbrance force, F_m , of grain boundary pinning exerted by second-phase particles [37] can be obtained using Equation (6):

$$F_m = \frac{3f\sigma}{2r}, \quad (6)$$

where r is the mean radius of MC, and valued as 25 nm and 10 nm for VC and V(C, N), respectively. The following result was obtained as shown in Table 5. It can be seen from the calculation that the incorporation of N into MC precipitates leads to a decrease in the interfacial energy of the MC/Fe matrix system. This suggests that the addition of nitrogen decreases the lattice misfit and the interfacial energy of MC with the austenite matrix and thereby hinders the movement of the austenite grain boundary efficiently. According to estimates, the contribution of V(C, N) on refining grains is 7.8 times of that of VC. i.e., nitrogen addition increases the grain refining efficiency of VC by 6.8 times. This result offers sound explanations as to why the size of prior austenitic grains in nitrogen-alloyed steel is smaller than in that of nitrogen-free steel. Comprehensive reasons for this inhibition ability may be that nitrogen addition not only increases the amount of MC carbides but also causes these carbides to be much finer and dispersed.

Table 5. Thermodynamic calculation results.

Precipitates	Lattice Mismatch (100%)	Interface Energy (J/m ²)	F_m (N/m ²)	$F_{m(V(C, N))}/F_{m(VC)}$
VC	0.1182	0.4449	5.6×10^4	7.8
V(C, N)	0.1122	0.4338	4.4×10^5	

4.3. Effect of Nitrogen on Martensitic Transformation

As is well known, added nitrogen has an effect on martensitic transformation [38]. The specific volume of martensite is bigger than that of austenite, an approximately volume expansion which is characterized by $\Delta l/l$ can be obtained when the martensite transformation is induced from supercooled austenite [39]. Therefore, transition temperatures of martensite can be obtained from the dilatometric curves by the tangent method. As shown in Figure 8, as the nitrogen-free sample is cooled at the rate of 25 °C/s, there is an abrupt change from 310 °C to 250 °C representing the martensite formation process in the tested steel. Therefore, M_S and M_f of the nitrogen-free steel can be inferred to be 310 °C and 250 °C, respectively. While, M_S and M_f are 280 °C and 175 °C for nitrogen-alloyed steel, respectively. Clearly, nitrogen addition decreases the transition temperature of martensitic greatly, increasing transformation resistance of martensitic. In other words, hardenability was significantly decreased by nitrogen. Remarkably, the decrease of M_S may increase the volume fraction of retained austenite, as shown in Figure 9. It is observed that the microstructure of both samples exhibits typical lath martensite, while the film-like retained austenite between martensitic lath in nitrogen-alloyed steel is more than that of nitrogen-free steel. Retained austenite in the microstructure can improve the resistance to impact fatigue by inhibiting the initiation and growth of fatigue crack, and increase the toughness of the steel [40]. However, owing to its relatively small volume fraction, the diffraction peak of austenite cannot be detected by XRD shown in Figure 6.

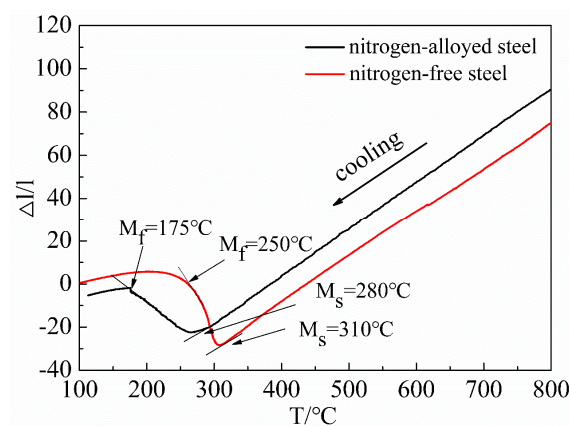


Figure 8. Transition temperatures of samples steels during quick cooling treatment (Δl and l are expansion length and original length of samples, respectively).

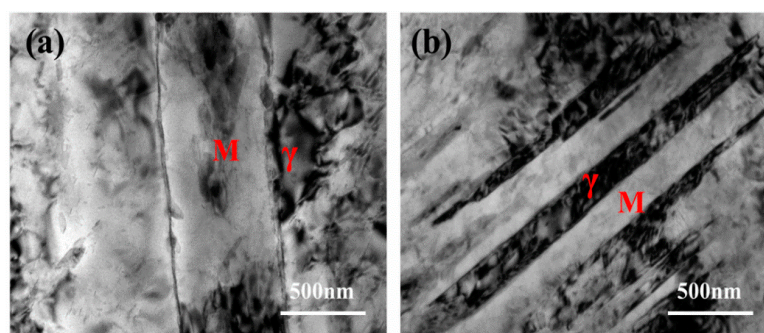


Figure 9. TEM micrographs of retained austenite in samples tempered at 600 °C for 4 h: (a) Nitrogen-free steel; (b) nitrogen-alloyed steel.

5. Conclusions

From the above-described experiment and theoretical analysis, the key points can be summarized as follows:

- (1) Nitrogen addition can increase hardness and temperability of 4Cr5Mo2V steel without toughness loss with a reasonable heat treatment procedure. The fair match of strength and high toughness of the nitrogen-alloyed 4Cr5Mo2V steel is associated with the refinement of the prior austenite grain size, the solution hardening of nitrogen atoms after tempering, and the increase of retained austenite.
- (2) During the heating stage of the quenching process, nitrogen promoted the precipitation of vanadium as finer V(C, N), imposing a stronger effect on restricting the growth of prior austenitic grains than VC and increasing grain refining efficiency of VC by 6.8 times. During the quenching process, the nitrogen decreases the M_s of the martensitic transformation, increasing retained austenite which is a benefit for toughness.
- (3) In the process of tempering, some of the N atoms in M(C, N) were dissolved in the matrix, causing crystal lattice distortions, thus boosting the solution reinforcing effect. Meanwhile, the solid-dissolved nitrogen inhibits the diffusion of carbon, decreasing the growth rate of the carbides, and increasing tempering resistance.

Acknowledgments: The authors acknowledge financial support from the National Natural Science Foundation of China (Grant No. U1660114 and Grant No. U51174026).

Author Contributions: Jinbo Gu and Jingyuan Li conceived and designed the experiments; Jinbo Gu performed the experiments; Jinbo Gu and Jingyuan Li analyzed the data; Yulai Chen was responsible for language modification; Jingyuan Li contributed reagents/materials/analysis tools; Jinbo Gu wrote the paper.

Conflicts of Interest: The authors declare no conflict of interest.

References

1. Gopalsamy, B.M.; Mondal, B.; Ghosh, S.; Arntz, K.; Klocke, F. Experimental investigations while hard machining of DIEVAR tool steel (50 HRC). *Int. J. Adv. Manuf. Technol.* **2010**, *51*, 853–869. [[CrossRef](#)]
2. Cong, D.L.; Zhou, H.; Ren, Z.N.; Zhang, Z.H.; Zhou, H.F.; Meng, C.; Wang, C.W. The thermal fatigue resistance of H13 steel repaired by a biomimetic laser remelting process. *Mater. Des.* **2014**, *55*, 597–604. [[CrossRef](#)]
3. Pérez, M.; Belzunce, F.J. The effect of deep cryogenic treatments on the mechanical properties of an AISI H13 steel. *Mater. Sci. Eng.* **2015**, *624*, 32–40. [[CrossRef](#)]
4. Silva, L.L.G.D.; Ueda, M.; Mello, C.B.; Codaro, E.N.; Lepienski, C.M. Effects of the high temperature plasma immersion ion implantation (PIII) of nitrogen in AISI H13 steel. *Mater. Sci.* **2008**, *43*, 5989–5997. [[CrossRef](#)]
5. Sola, R.; Giovanardi, R.; Parigi, G.; Veronesi, P. A novel method for fracture toughness evaluation of tool steels with post-tempering cryogenic treatment. *Metals* **2017**, *7*, 75. [[CrossRef](#)]
6. Podgornik, B.; Paulin, I.; Zajec, B.; Jacobson, S.; Leskovšek, V. Deep cryogenic treatment of tool steels. *J. Mater. Process. Technol.* **2016**, *229*, 398–406. [[CrossRef](#)]
7. Kheirandish, S.; Noorian, A. Effect of niobium on microstructure of cast AISIH13 hot work tool steel. *J. Iron Steel Res. Int.* **2008**, *15*, 61–66. [[CrossRef](#)]
8. Wang, M.; Dangshen, M.A.; Liu, Z.; Zhou, J.; Chi, H.; Dai, J. Effect of Nb on segregation, primary carbides and toughness of H13 steel. *Acta Metall. Sin.* **2014**, *50*, 285–293.
9. Gao, J.Z.; Fu, P.X.; Liu, H.W.; Li, D.Z. Effects of rare earth on the microstructure and impact toughness of H13 Steel. *Metals* **2015**, *5*, 383–394. [[CrossRef](#)]
10. Schino, A.D.; Barteri, M.; Kenny, J.M. Grain size dependence of mechanical, corrosion and tribological properties of high nitrogen stainless steels. *J. Mater. Sci.* **2003**, *38*, 3257–3262. [[CrossRef](#)]
11. Hänninen, H.; Romu, J.; Ilola, R.; Laitinen, A. Effects of processing and manufacturing of high nitrogen-containing stainless steels on their mechanical, corrosion and wear properties. *J. Mater. Process. Technol.* **2001**, *117*, 424–430. [[CrossRef](#)]

12. Jung, J.G.; Bae, J.H.; Lee, Y.K. Quantitative evaluation of dynamic precipitation kinetics in a complex Nb-Ti-V microalloyed steel using electrical resistivity measurements. *Met. Mater. Int.* **2013**, *19*, 1159–1162. [[CrossRef](#)]
13. Simmons, J.W. Overview: High-Nitrogen Alloying of Stainless. *Mater. Sci. Eng.* **1996**, *207*, 159–169. [[CrossRef](#)]
14. Werner, E. Solid solution and grain size hardening of nitrogen-alloyed austenitic steels. *Mater. Sci. Eng.* **1988**, *101*, 93–98.
15. Behjati, P.; Kermanpur, A.; Najafizadeh, A. Influence of nitrogen alloying on properties of Fe318Cr312Mn3XN austenitic stainless steels. *Mater. Sci. Eng.* **2013**, *588*, 43–48. [[CrossRef](#)]
16. Gu, J.B.; Li, J.Y.; Huo, J.H. Effect of precipitation on hardening and toughening of nitrogen-alloyed H13 steel. *Steel Res. Int.* **2017**. [[CrossRef](#)]
17. SISC IAS, version 8.0; Scientific Instrument Software Co. Ltd.: Beijing, China, 2003.
18. ASTM. *Standard Test Methods for Determining Average Grain Size*; ASTM E 112-10; ASTM International: West Conshohocken, PA, USA, 2010.
19. Ning, A.G.; Guo, H.J.; Chen, X.C. Precipitation behaviors and strengthening of carbides in H13 steel during annealing. *Mater. Trans.* **2015**, *56*, 581–586.
20. Chen, C.; Zhang, F.C.; Yang, Z.N.; Zheng, C.L. Superhardenability behavior of vanadium in 40CrNiMoV steel. *Mater. Des.* **2015**, *83*, 422–430. [[CrossRef](#)]
21. Wang, T.S.; Zhang, M.; Wang, Y.H.; Yang, J.; Zhang, F.C. Martensitic transformation behaviour of deformed supercooled austenite. *Scr. Mater.* **2013**, *68*, 162–165. [[CrossRef](#)]
22. Xu, L.Q.; Zhang, D.T.; Liu, Y.C.; Ning, B.Q. Precipitation behavior and martensite lath coarsening during tempering of T/P92 ferritic heat-resistant steel. *Int. J. Min. Met. Mater.* **2014**, *21*, 438–447. [[CrossRef](#)]
23. Wang, Z.Q.; Zhang, H.; Guo, C.H.; Jiang, F.C. Effect of molybdenum addition on the precipitation of carbides in the austenite matrix of titanium micro-alloyed steels. *J. Mater. Sci.* **2016**, *51*, 4996–5007. [[CrossRef](#)]
24. Zagonel, L.F.; Bettini, J.; Basso, R.L.O.; Paredez, P. Nanosized precipitates in H13 tool steel low temperature plasma nitriding. *Surf. Coat. Technol.* **2012**, *207*, 72–78. [[CrossRef](#)]
25. Chen, Y.L.; Liu, B.; Li, J.Y. Study on heat treatment of nitrogen H13 steel. *Adv. Mater. Res.* **2010**, *146*, 1885–1888. [[CrossRef](#)]
26. Li, J.Y.; Chen, Y.L.; Huo, J.H. Mechanism of improvement on strength and toughness of H13 die steel by nitrogen. *Mater. Sci. Eng.* **2015**, *640*, 16–23. [[CrossRef](#)]
27. Gavriljuk, V.G. Nitrogen in Iron and Steel. *ISIJ Int.* **1996**, *36*, 738–745. [[CrossRef](#)]
28. Xie, Y.; Cheng, G.G.; Chen, L.; Zhang, Y.D.; Yan, Q.Z. Characteristics and Generating Mechanism of Large Precipitates in Nb-Ti-microalloyed H13 Tool Steel. *ISIJ Int.* **2016**, 995–1002. [[CrossRef](#)]
29. Michaud, P.; Delagnes, D.; Lamesle, P.; Mathon, M.H.; Levaillant, C. The effect of the addition of alloying elements on carbide precipitation and mechanical properties in 5% chromium martensitic steels. *Acta Mater.* **2007**, *55*, 4877–4889. [[CrossRef](#)]
30. Huang, B.X.; Wang, C.Z.; Wang, X.Y.; Rong, Y.H. Effect of nitrogen on martensitic transformation and mechanical properties of TWIP steel. *Acta Metall. Sin.* **2012**, *48*, 769–774. [[CrossRef](#)]
31. Song, W.W.; Radulescu, A.; Liu, L.L.; Bleck, W. Study on a high entropy alloy by high energy synchrotron X-Ray diffraction and small angle neutron scattering. *Steel Res. Int.* **2017**. [[CrossRef](#)]
32. Moon, J.; Lee, T.H.; Shin, J.H.; Lee, J.W. Hot working behavior of a nitrogen-alloyed Fe-18Mn-18Cr-N austenitic stainless steel. *Mater. Sci. Eng.* **2014**, *594*, 302–308. [[CrossRef](#)]
33. Saklakoğlu, N. Characterization of surface mechanical properties of H13 steel implanted by plasma immersion ion implantation. *J. Mater. Process. Technol.* **2007**, *189*, 367–373. [[CrossRef](#)]
34. Delagnes, D.; Lamesle, P.; Mathon, M.H.; Mebarki, N.; Levaillant, C. Influence of silicon content on the precipitation of secondary carbides and fatigue properties of a 5% Cr tempered martensitic steel. *Mater. Sci. Eng.* **2005**, *394*, 435–444. [[CrossRef](#)]
35. Xue, S.; Zhou, J.; Zhang, Y.W.; Geng, P. Analysis of carbides in spheroidized H13 steel. *Trans. Mater. Heat Treat.* **2012**, *33*, 100–105.
36. Kang, M.; Park, G.; Jung, J.G.; Kim, B.H.; Lee, Y.K. The effects of annealing temperature and cooling rate on carbide precipitation behavior in H13 hot-work tool steel. *J. Alloys Compd.* **2015**, *627*, 359–366. [[CrossRef](#)]
37. Yong, Q.L. *Secondary Phases in Steels*, 1st ed.; Metallurgical Industry Press: Beijing, China, 2006; pp. 228–247. (In Chinese)

38. Prokoshkina, V.; Kaputkina, L. Peculiarities of martensitic transformations and martensite structure in high nitrogen steels. *Mater. Sci. Eng.* **2007**, *481*, 762–765. [[CrossRef](#)]
39. Yang, H.S.; Bhadeshia, H.K.D.H. Uncertainties in dilatometric determination of martensite start temperature. *Mater. Sci. Technol.* **2007**, *23*, 556–560. [[CrossRef](#)]
40. Lacroix, G.; Pardoën, T.; Jacques, P.J. The fracture toughness of TRIP-assisted multiphase steels. *Acta Mater.* **2008**, *56*, 3900–3913. [[CrossRef](#)]



© 2017 by the authors. Licensee MDPI, Basel, Switzerland. This article is an open access article distributed under the terms and conditions of the Creative Commons Attribution (CC BY) license (<http://creativecommons.org/licenses/by/4.0/>).